

SAM-OCTA: Prompting Segment-Anything for OCTA Image Segmentation

Xinrun Chen^a, Chengliang Wang^{a,*}, Haojian Ning^a and Shiyong Li^b

^aCollege of Computer Science, Chongqing University, No.174 Shazheng St., Shapingba District, Chongqing, 400044, China

^bXiang'an Hospital of Xiamen University, No.2000, Xiang'an East Road, Xiamen, 361104, China

ARTICLE INFO

Keywords:

Optical Coherence Tomography Angiography
Image Segmentation
Model Fine-tuning
Prompt Point

ABSTRACT

In the analysis of optical coherence tomography angiography (OCTA) images, the operation of segmenting specific targets is necessary. Existing methods typically train on supervised datasets with limited samples (approximately a few hundred), which can lead to overfitting. To address this, the low-rank adaptation technique is adopted for foundation model fine-tuning and proposed corresponding prompt point generation strategies to process various segmentation tasks on OCTA datasets. This method is named SAM-OCTA and has been experimented on the publicly available OCTA-500 and ROSE datasets. This method achieves or approaches state-of-the-art segmentation performance metrics. The effect and applicability of prompt points are discussed in detail for the retinal vessel, foveal avascular zone, capillary, artery, and vein segmentation tasks. Furthermore, SAM-OCTA accomplishes local vessel segmentation and effective artery-vein segmentation, which was not well-solved in previous works. The code is available at <https://github.com/ShellRedia/SAM-OCTA>.

1. Introduction

Optical Coherence Tomography Angiography (OCTA) is an innovative and non-invasive imaging technique that enables the visualization of retinal microvasculature with high resolution and without needing dye injection (Wang, Shen, Yuan, Xu, Yang, Liu, Cai, Cheng and Wang, 2021). This extension of Optical Coherence Tomography (OCT) provides qualitative and quantitative information about blood flow contrast in various retinal layers, making it a valuable tool for disease staging and preclinical diagnosis, including diabetic retinopathy and age-related macular degeneration (Liang, Zhang and An, 2021; López-Varela, de Moura, Novo, Fernández-Vigo, Moreno-Morillo and Ortega, 2023). Due to its non-invasive nature and quick image acquisition, OCTA has gained popularity in ophthalmology, and its applications have expanded to other medical fields, such as dermatology (Li, Zeghlache, Brahim, Xu, Tan, Conze, Lamard, Quellec and El Habib Daho, 2022b; López-Varela et al., 2023).

However, OCTA faces challenges related to image quality variation caused by factors like patient cooperation, media opacity, and motion artifacts (Wang et al., 2021; Breger, Goldbach, Gerendas, Schmidt-Erfurth and Ehler, 2022). The specific retinal structures, such as the retinal vessels (RVs) and foveal avascular zone (FAZ), have been targeted for segmentation to aid in the detection and monitoring of retinal diseases (Liang et al., 2021; Hu, Jiang, Zhang, Li and Gao, 2022b; Li, Zhang, Li and Wang, 2022a). Some computer-aided diagnosis (CAD) systems have also been developed, contributing to the clinical evaluation of various ophthalmic diseases (López-Varela et al., 2023; Vali, Nazari, Sadri, Pour,

Riazi-Esfahani, Faghihi, Ebrahimiadib, Azizkhani, Innes, Steel et al., 2023; Meiburger, Salvi, Rotunno, Drexler and Liu, 2021). Researchers have been actively exploring deep learning-based methods for image quality assessment and segmentation with limited datasets to address these challenges and enhance the accuracy and efficiency of OCTA image analysis.

Most deep learning segmentation methods related to OCTA are based on self-designed neural networks and modules. This requires training the model from scratch, which can lead to overfitting issues, especially in the case of small datasets like OCTA. Foundational models have revolutionized artificial intelligence (AI) with extensive pre-training on web-scale datasets and powerful generalization. In various AI areas, including computer vision and NLP, large AI models are actively researched, fostering future advancements and breakthroughs (Zhang, Liu, Cui, Huang, Lin, Yang and Hu, 2023; Shi, Qiu, Abaxi, Wei, Lo and Yuan, 2023a).

Segment Anything Model (SAM) was introduced as a foundational model for addressing natural image tasks. This foundational model demonstrated the promising wide applicability to various image segmentation tasks for the first time without needing prior re-training (Kirillov, Mintun, Ravi, Mao, Rolland, Gustafson, Xiao, Whitehead, Berg, Lo et al., 2023). In addition to excelling in natural image processing, SAM has emerged as a promising model in medical image segmentation. Accurately identifying anatomical structures and lesions is crucial for an effective medical segmentation model. (Cheng, Qin, Jiang, Zhang, Lao and Li, 2023). However, applying SAM to medical image segmentation presents its own set of challenges. Medical images differ significantly from natural images in quality, noise, resolution, and other factors, affecting SAM's segmentation performance. Thus, further research and optimization efforts are required to harness SAM's potential in medical image segmentation fully (Zhang and Jiao, 2023).

*Corresponding author

✉ chenxinrun@cqu.edu.cn (X. Chen); wangcl@cqu.edu.cn (C. Wang);
nhj@cqu.edu.cn (H. Ning); shiyong_li@126.com (S. Li)
ORCID(s): 0000-0001-8982-9330 (X. Chen)

Adopting a fine-tuning approach to SAM and introducing prompt information can enhance and guide the model's segmentation, aiming to improve some complex OCTA segmentation cases. We summarize the contributions of this paper as follows:

- a) We employ the SAM model, a pre-trained foundational model with prompt information, for the segmentation task of OCTA images for the first time. The fine-tuned model has been tested on multiple OCTA datasets, achieving or approaching the results at the state-of-the-art level.
- b) We fine-tune the parameters of SAM using OCTA datasets and the LoRA (Low-Rank Adaptation) method. This fine-tuning process aims to adapt SAM to the segmentation task on OCTA images while preserving its solid semantic understanding of images.
- c) We propose a prompt point generation strategy for OCTA image segmentation tasks and conduct a comprehensive experimental analysis of the effectiveness of prompt points in RV, FAZ, capillary and artery-vein segmentation tasks.

2. Related Work

2.1. OCTA Segmentation Models

As a typical architecture for deep image processing, the vision transformer (ViT) is frequently used for segmentation tasks in OCTA (Dosovitskiy, Beyer, Kolesnikov, Weissenborn, Zhai, Unterthiner, Dehghani, Minderer, Heigold, Gelly et al., 2020). Shi, Li, Zou and Zhang (2023b) proposes an efficient Cross-Fusion transformer to achieve continuous vessel segmentation, addressing issues like vessel discontinuities or missing segments while maintaining linear computational complexity. OCT2Former is a hybrid Transformer-based approach for retinal OCTA vessel segmentation. By utilizing multi-head dynamic label aggregation attention in a dynamic label aggregation transformer, OCT2Former captures global retinal vessel information while reducing computational complexity (Tan, Chen, Meng, Shi, Xiang, Chen, Pan and Zhu, 2023). StruNet (Swin Transformer-based Residual U-Net) is another novel encoder-decoder architecture used for general medical image denoising, incorporating the Swin-Transformer to improve denoising effectiveness (Ma, Yan, Liu, Liu, Zhang and Zhao, 2023).

The above method is sufficient to demonstrate the effectiveness and potential of the ViT-based SAM in OCTA images. More supervised segmentation methods are proposed, typically following a coarse-to-fine feature extraction process. IPN (Image Projection Network) is a 3D-to-2D segmentation network for OCTA images and presents a projection learning module that enables effective feature selection and dimension reduction (Li, Chen, Ji, Xie, Yuan, Chen and Li, 2020a). Another approach presents a novel split-based coarse-to-fine RV segmentation network for OCTA images, demonstrating robust and accurate vessel segmentations on various types of retinal images (Ma, Hao,

Xie, Fu, Zhang, Yang, Wang, Liu, Zheng and Zhao, 2020). The OVS-Net (OCTA Vessel Segmentation Network) adopts a two-stage cascaded structure to process OCTA images and provide continuous probability maps for vessel segmentation (Zhu, Wang, Xiao, Dai, Liu and Zou, 2022). The RPS-Net (retinal image projection segmentation network) consists of parallel modules for learning global semantic features and incorporating local details from the volumetric data to obtain more accurate segmentation results (Li et al., 2022a). The DB-UNet architecture introduces a dual-branch MLP-Mixer segmentation technique, which has been proven effective in accurately segmenting RVs with low computational complexity (Wang, Ning, Chen and Li, 2023).

Furthermore, the recent rise of unsupervised methods has led to some research applying relevant techniques to OCTA images (He, Fan, Wu, Xie and Girshick, 2020; Liu, Shen, Wang, Kang and Tian, 2021). These methods can extract certain features across datasets, enabling segmentation or denoising tasks to be accomplished (Liang et al., 2021; Wu, Gao, Williams, Stylianides, Zheng and Jin, 2020; Ma, Feng, Wang and Ma, 2022).

The abovementioned methods have demonstrated precise RVs and FAZ segmentation in OCTA images. However, more complex tasks, such as artery-vein segmentation, face challenges and often result in vessel misclassifications and segmentation region discontinuities.

2.2. Fine-tuning Approaches

The SAM is a foundational vision model for general image segmentation. With the ability to segment diverse objects, parts, and visual structures in various scenarios, SAM inputs prompt like points, bounding boxes, or coarse masks. Its remarkable zero-shot segmentation capabilities enable its easy transfer to numerous applications through simple prompting (Kirillov et al., 2023; Liu, He, Kang, Zhuang, Wang and Xu, 2023).

Although SAM has established an efficient data engine for model training, relatively few cases are collected for medical applications or other rare image scenarios. Therefore, some fine-tuning methods have been applied to SAM to improve its performance in certain segmentation failure cases. The SAMed (SAM for Medical) adopts the low-rank-based fine-tuning strategy (LoRA) to approximate the low-rank updates of the parameters in the image encoder. It also fine-tunes the lightweight prompt encoder and the mask decoder of SAM, resulting in improved organ segmentation performance (Hu, Shen, Wallis, Allen-Zhu, Li, Wang, Wang and Chen, 2021; Zhang and Liu, 2023). HQ-SAM (High-Quality SAM) achieves fine-tuning by improving the decoder, enabling SAM to predict highly accurate segmentation masks even in challenging scenarios, such as grids on the tennis racket (Ke, Ye, Danelljan, Liu, Tai, Tang and Yu, 2023). Another approach, named SAM-PARSER (SAM-PARAmeter SpAcE Reconstruction), analyzes SAM's parameter space in the new dataset through matrix decomposition and fine-tuning the coefficients using the optimal

linear combination of the parameter space's base (Peng, Xu, Zeng, Yang and Shen, 2023).

The common characteristic of these fine-tuning methods is only adding a small number of trainable parameters when processing the new datasets. The advantage of fine-tuning methods is preserving the SAM's strong zero-shot capabilities and flexibility and extending its capability for high-quality segmentation in a new segmentation task.

2.3. Artery-Vein Segmentation

Retinal arteries and veins are small blood vessels associated with various eye and systemic diseases (Cheung, Ikram, Klein and Wong, 2015). Diseases impact arteries and veins differently. For instance, increased arteriolar tortuosity is linked to diabetic retinopathy, while widened venular caliber is associated with the risk of ischemic stroke. Hence, extracting and distinguishing retinal arteries and veins is crucial for their diagnostic significance (Cheung, Sabanayagam, Law, Kumari, Ting, Tan, Mitchell, Cheng and Wong, 2017; Seidelmann, Claggett, Bravo, Gupta, Farhad, Klein, Klein, Di Carli and Solomon, 2016). Some methods have been investigated for this problem in fundus and OCTA images. These include the use of convolutional neural networks, graph neural networks, and generative adversarial networks for segmentation purposes (Mishra, Wang, Wei, Chen and Hu, 2021; Hu, Wang, Wu, Cao, Mou, Zhao and Zhang, 2022a; Alam, Le, Son, Lim and Yao, 2020).

Due to the morphological similarities between retinal arteries and veins and the complexities introduced by factors such as age, gender, and disease conditions, deep learning methods often encounter segmentation disconnections or confusion in the artery-vein segmentation task. However, SAM can effectively address these challenges with the ability to incorporate positional prompts for precise segmentation of specific targets in the same image.

3. Method

In this paper, we fine-tune the pre-trained SAM using OCTA datasets and corresponding annotations. The proposed method is named SAM-OCTA, and the flowchart in Figure 1 illustrates the process. SAM consists of three parts: an image encoder, a flexible prompt encoder, and a fast mask decoder (Kirillov et al., 2023). The types of segmentation tasks can be divided into global and local.

3.1. Fine-tuning of Image Encoder

The image encoder utilizes a ViT pre-trained with the masked auto-encoder (MAE) method. The chosen ViT model comes in three variants: vit-b, vit-h, and vit-l, which can only process fixed-size inputs (e.g. $1024 * 1024 * 3$). Scaling and padding operations are employed to support input images of different resolutions. In this study, we employed the image encoder from the "vit-h" model for the fine-tuning process.

As shown in Figure 2, OCTA data is inherently in 3D format, but most datasets provide en-face 2D projection

forms. These 2D images are obtained by layer-wise segmentation based on anatomical structures, which preserves the integrity of vascular structures well. As SAM requires three-channel images as input, in this work, we stack projection layers in different depths of OCTA images to adapt to this input format. The benefit of this approach is that it preserves the vascular structure information in the OCTA images while fully utilizing SAM's feature-extracting capabilities.

Fine-tuning aims to retain SAM's powerful image understanding capabilities while enhancing its performance on OCTA, which is an uncommon image format. The approach used in this paper involves utilizing the LoRA technique (Hu et al., 2021), which introduces additional linear network layers in each transformer block of SAM, similar in form to a ResNet block. During the training process, the weights of the image encoder are frozen, and only the newly introduced parameters are updated. The fine-tuning process can be described as Algorithm 1.

Algorithm 1 Fine-tuning of SAM

Require:

- sam*: SAM
 - r*: rank of LoRA
 - x_i : input image of OCTA sample
 - x_p : prompt points coordinates of OCTA sample
 - y_{label} : segmentation ground-truth of OCTA sample
 - 1: Freeze the parameters of SAM's modules.
 - 2: Pre-process the input image x_i as x .
 - 3: **for** *block* in *sam.ImageEncoder.AttentionBlocks* **do**
 - 4: $d = block.qkv.dim$ // number of dimensions of qkv matrix
 - 5: $l_{qa} = l_{va} = Linear(d, r)$
 - 6: $l_{qb} = l_{vb} = Linear(r, d)$
 - 7: $y_1 = block.qkv(x)$
 - 8: $y_q = l_{qb}(l_{qb}(x))$
 - 9: $y_v = l_{vb}(l_{vb}(x))$
 - 10: $x = y_1 + y_q + y_v$ // assign x for next iteration
 - 11: **end for**
 - 12: $z_i = x$ // latent feature of input image
 - 13: $z_p = sam.PromptEncoder(x_p)$ //convert prompt points coordinates to embeddings
 - 14: Merge z_i and z_p as z_d .
 - 15: $y_{mask} = sam.MaskDecoder(z_d)$
 - 16: Post-process the predicted mask y_{mask} .
 - 17: Calculate the loss function based on y_{label} and y_{mask} , and update the parameters of the LoRA module.
-

3.2. Prompt Points Generation Strategy

The prompt encoder is divided into two types of prompts: sparse prompts (points, boxes, text) and dense prompts (masks). For sparse prompts, position encodings are used to represent points and boxes, and these position encodings are added to the learned embeddings of each prompt type. For free-form text, the pre-trained text encoder from CLIP is utilized (Radford, Kim, Hallacy, Ramesh, Goh, Agarwal, Sastry, Askell, Mishkin, Clark et al., 2021). As for dense

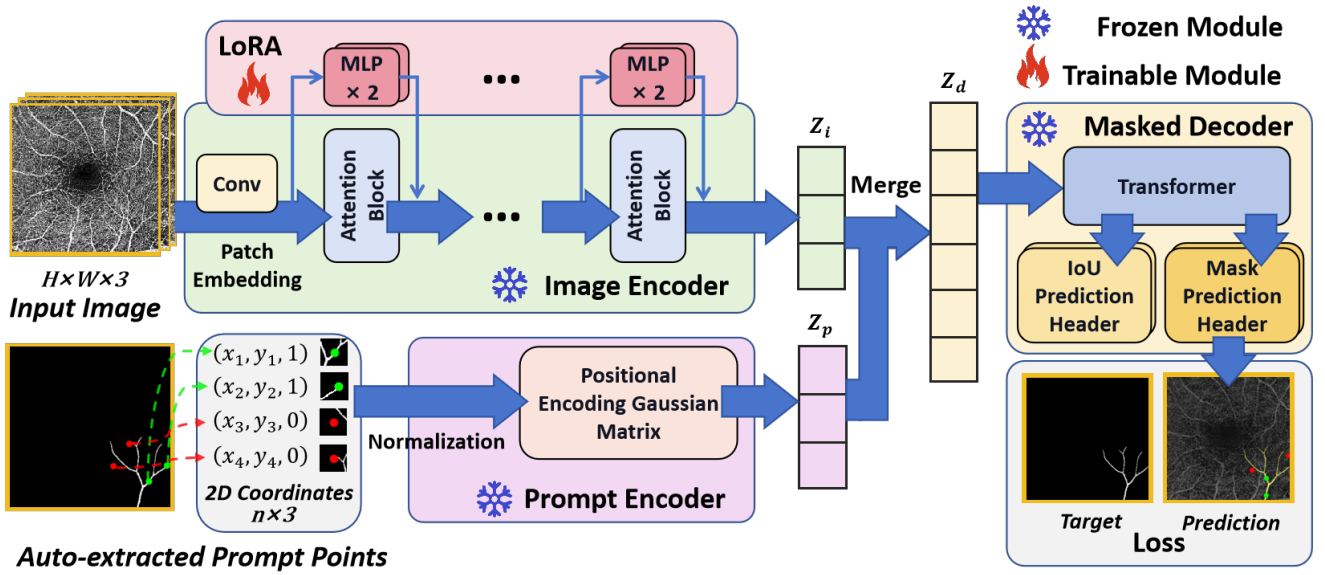


Figure 1: Schematic diagram illustrating the fine-tuning of SAM using OCTA samples.

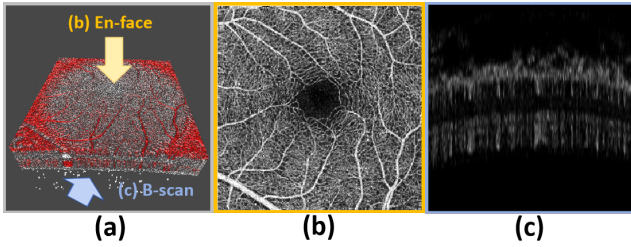


Figure 2: OCTA structural diagram. (a) Three-dimensional volume rendering with arrows indicating different projection directions. (b) En-face projection. (c) B-scan.

prompts (masks), convolutional operations are applied for embedding, and the resulting embeddings are element-wise summed with the image embeddings. In our work, we chose points as the prompt for the segmentation tasks. This prompt method is the most intuitive, while other prompt methods are challenging to apply to OCTA segmentation tasks.

For each sample's prompt point input, assuming there are N points in the prompt point input, it can be represented as: $(x_1, y_1, 1), (x_2, y_2, 1), \dots, (x_{n-1}, y_{n-1}, 0), (x_n, y_n, 0)$, where 1 and 0 represent the positive and negative types of prompt points, respectively, corresponding to the foreground and background of the segmentation. The prompt encoder of SAM will perform embedding on this input, and due to its pre-training, it can appropriately integrate with the information from the image encoder. Since the OCTA image samples' segmentation labels can be viewed as a bipartite graph, foreground and background can be randomly sampled at different positions to input the prompt encoder. The purpose of randomly generating points is to simulate user prompt operations and increase the model's generalization

ability. This random point sampling strategy applies to the FAZ, RV, and capillary segmentation, similar to the segmentation methods listed in Section 2.1. When selecting negative points for artery-vein segmentation, it is necessary to select some negative points in non-target vascular areas to strengthen the distinction between the two types of vessels is also necessary.

As a local segmentation task, the task of segmenting individual vessels separately has not been attempted in previous works. By incorporating the prompt encoder, more accurate local vessel segmentation can be achieved in OCTA datasets. For this task, the first step is to identify and label all connected components in the segmentation masks and distinguish them by assigning unique identifiers. Due to the weak connectivity at the endpoints of some vessels in OCTA labels, we adopt the eight-connectivity criterion. The prompt points generation process can be described as Algorithm 2 and Figure 3.

3.3. Mask Decoder

The role of the mask decoder is to efficiently map the image embeddings, prompt embeddings, and output tokens to a segmentation mask. A modified version of the transformer decoder block is employed, followed by a dynamic mask prediction head. The mask decoder outputs multiple segmentation masks to represent objects at different semantic levels for image input and corresponding prompt input. In this work, the loss function involved in the fine-tuning process is computed based on the segmentation output with the highest confidence score.

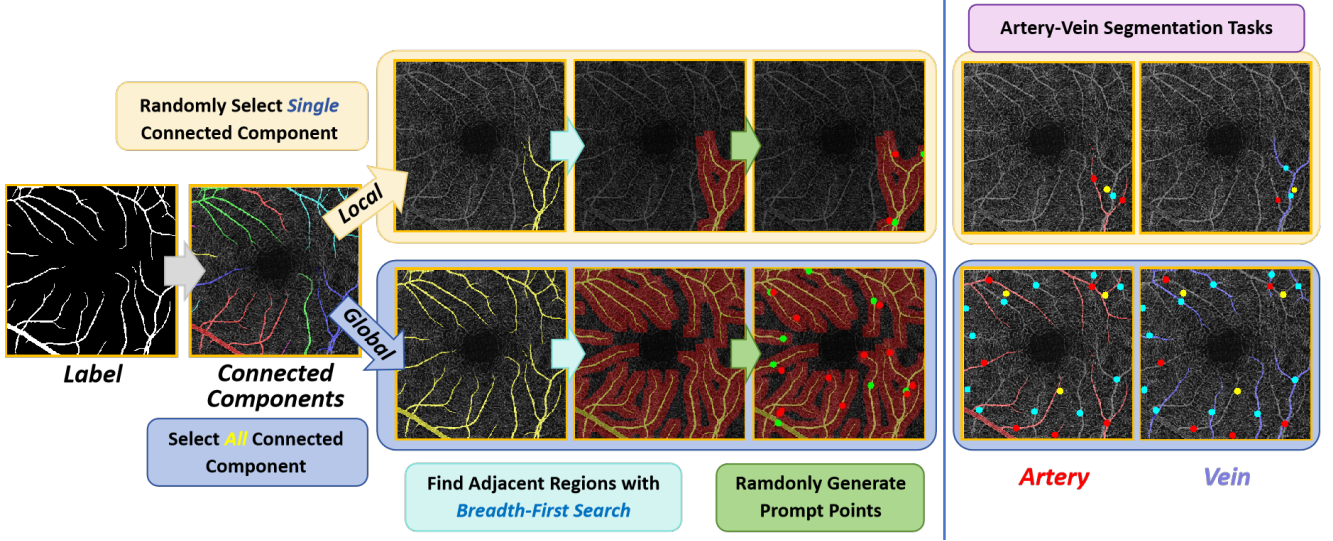


Figure 3: Schematic diagram of prompt points generation. For RV, FAZ, and capillary segmentation, green represents positive points, and red represents negative points. The red area in the figure represents the region where negative points can be selected. For artery-vein segmentation, to highlight the difference between arteries and veins, red is used to represent the artery regions, and blue is the vein regions. The color of the prompt points is adjusted accordingly: red for arteries, cyan for veins, and yellow for non-vessel background. For the artery segmentation tasks, red points are positive, and the rest are negative, while cyan points are positive for the vein.

Table 1
Summary of the OCTA datasets.

Dataset	Size	FoV	Label						Center
			RV	FAZ	Capillary	Artery	Vein	-line	
OCTA-500	500	3M/6M	✓	✓	✓	✓	✓	✗	
ROSE	39	3M	✓	✓	✓	✗	✗	✓	

4. Experiments

4.1. Datasets and Preprocessing

The publicly available datasets used in this paper are OCTA-500 and ROSE (Li, Zhang, Ji, Xie, Yuan, Liu and Chen, 2020b; Hao, Shen, Zhu, Liu, Behera, Zhang, Chen, Liu, Zhang and Zhao, 2022). The targets are segmented from the en-face projection images in this study. The OCTA-500 dataset contains 500 samples, classified based on the field of view (FoV) with two scales: $3mm * 3mm$ (3M) and $6mm * 6mm$ (6M). The corresponding image resolutions are $304 * 304$ and $400 * 400$, with 200 and 300 samples respectively. Compared to the 3M images, the vessels in the 6M images are more complicated and correspond to a broader range of possible disease types. The ROSE dataset includes 39 OCTA images with FoV of 3M. The OCTA-500 dataset annotates FAZ, RV, capillary, artery, and vein. The ROSE dataset annotates FAZ, RV, and capillary. For the RV, centerline annotations are also provided. The information on the experimental datasets used is summarized in Table 1.

The adopted data augmentation tool is Albumentations, which offers Spatial- and pixel-level image transforms

(Buslaev, Iglovikov, Khvedchenya, Parinov, Druzhinin and Kalinin, 2020). The data augmentation strategies for OCTA images include horizontal flipping, brightness and contrast adjustment, and random slight rotation (-10 to 10 degrees), which enhance the model's generalization. The SAM requires input images with three channels. For the OCTA-500 and ROSE datasets, as each sample contains different depth scan layers, we merge them into three-channel images.

4.2. Experimental Settings

The SAM is deployed on A100 graphic cards with 80 GB of memory. The 10-fold cross-validation is adopted to evaluate the training results. The number of training epochs is 50. The optimizer used is AdamW, and the learning rate is set using a warm-up strategy, which can be expressed as:

$$lr = \begin{cases} \frac{t}{10^4}, & t \leq 10 \\ \max(\frac{1}{10^5}, \frac{1}{10^{3+0.98*(t-10)}}), & t > 10 \end{cases} \quad (1)$$

where,

$lr \rightarrow$ learning rate,

$t \rightarrow$ current training epoch.

The loss functions used for fine-tuning vary depending on the segmentation tasks. For FAZ and capillary, the Dice loss is employed. However, for RV, artery, and vein, the cDice loss is utilized (Shit, Paetzold, Sekuboyina, Ezhov, Unger, Zhylka, Pluim, Bauer and Menze, 2021). Accurate segmentation of tubular, network-like structures, such as RV, neuron, or road, is relevant to the centerline. There are two steps to calculate the cDice loss. The cDice loss can leverage this topological property to assist in preserving the

Algorithm 2 Prompt Points Generation

Require:

y_{label} : label of the OCTA sample
 N_{pos}, N_{total} : number of positive/total prompt points
 $isLocal$: generation mode

Ensure:

x_p : generated prompt points
 1: Extract all connected components from the y_{label} (e.g. using the Scipy library).
 2: Remove small connected components according to area.
 3: Let x_{pos}/x_{neg} be the sets of coordinates of the positive/negative prompt points.
 4: **if** $isLocal$ is *True* **then**
 5: Randomly select a connected component as c .
 6: Perform breadth-first search to obtain the neighboring region of c as c' .
 7: Randomly select N_{pos} positive points from c and $N_{total} - N_{pos}$ negative points from c' .
 8: Adding the prompt points to the sets x_{pos}/x_{neg} .
 9: **else**
 10: **for** c in connected components **do**
 11: Randomly selecting N_{pos} positive prompt points from the set of coordinates within c .
 12: Add the point to the set x_{pos} .
 13: **end for**
 14: Performing breadth-first search to obtain the neighboring region of the union of c as c' .
 15: Randomly selecting $N_{total} - x_{pos.size}$ negative points from c' .
 16: **end if**
 17: Concatenating x_{pos} and x_{neg} to form x_p .

connectivity of tubular segmentations. First, min- and max-pooling layers are used to iteratively extract the centerline of the predicted image and the label, similar to the erosion operation in morphology (it is given for the ROSE dataset, and this step can be skipped). Then, based on the predicted values, labels, and the extracted centerline, the cIDice loss can be calculated. These two loss functions can be represented as:

$$L_{Dice} = 1 - \frac{2 * |\hat{Y} \cap Y|}{|\hat{Y}| + |Y|}, \quad (2)$$

$$T_{prec}(\hat{Y}_s, Y) = \frac{|\hat{Y}_s \odot Y| + \epsilon}{|\hat{Y}_s| + \epsilon}, \quad (3)$$

$$T_{sens}(Y_s, \hat{Y}) = \frac{|Y_s \odot \hat{Y}| + \epsilon}{|Y_s| + \epsilon}, \quad (4)$$

$$L_{clDice} = 1 - 2 * \frac{T_{prec}(\hat{Y}_s, Y) * T_{sens}(Y_s, \hat{Y})}{T_{prec}(\hat{Y}_s, Y) + T_{sens}(Y_s, \hat{Y})}, \quad (5)$$

where

$Y \rightarrow$ the ground-truth,
 $\hat{Y} \rightarrow$ the predicted value,
 $Y_s, \hat{Y}_s \rightarrow$ soft-skeleton(Y, \hat{Y}),
 $\epsilon \rightarrow 10^{-6}$.

Experiments conducted in previous studies have shown that using only the cIDice loss can lead to the failure of the model training. In practical applications, it is necessary to use a weighted combination of cIDice loss and Dice loss for effective results:

$$L_{clDice} = 0.8 * L_{Dice} + 0.2 * L'_{clDice}. \quad (6)$$

4.3. Results

We conducted extensive experiments with various cases on multiple OCTA datasets. The segmentation results using metrics Dice, Jaccard, and Hausdorff Distance (HD), which are calculated as follows:

$$Dice(\hat{Y}, Y) = \frac{2|\hat{Y} \cap Y|}{|\hat{Y}| + |Y|}, \quad (7)$$

$$Jaccard(\hat{Y}, Y) = \frac{|\hat{Y} \cap Y|}{|\hat{Y} \cup Y|}, \quad (8)$$

$$HD(\hat{Y}, Y) = \max(h(\hat{Y}, Y), h(Y, \hat{Y})), \quad (9)$$

$$h(\hat{Y}, Y) = \max_{\hat{y} \in \hat{Y}} \min_{y \in Y} ||\hat{y} - y||. \quad (10)$$

4.3.1. Global Mode

The targets for the segmentation tasks that use the global mode to generate prompt points include RV, FAZ, capillary, artery, and vein. The distribution and size of the targets in the image vary for each segmentation task, therefore, the number of prompt points also differs. The experimental results are summarized in Table 2. The setting of prompt points depends on the number of connected components in the labels. The number of connected components varies among different samples. Our strategy is to initially assign a fixed number of positive points to each connected component and then add several negative points in the background region to maintain an equal total number of points. The purpose of doing this is to provide the prompt encoder with input tensors of the same size. In 5.1, We have provided a more detailed explanation of the number of feature points for different tasks.

From Table 2 and Figure 4, 5, it can be observed that for RV and capillary segmentation, there is only a slight improvement in the metrics after adding prompt points. From the test segmented samples, it is inferred that such results occur because vessels in OCTA images have a widespread distribution and slender shapes. In this case, the impact

Table 2

Segmentation results for the global mode.

Label	Dataset	Prompt Points		Dice ↑	Jaccard ↑	HD ↓
		Positive	Total			
RV	OCTA-500(3M)	0	0	0.9165	0.8431	4.1843
		1	20	0.9164	0.8460	4.1260
		2	40	0.9199	0.8520	4.1056
	OCTA-500(6M)	0	0	0.8865	0.7955	5.3860
		1	20	0.8869	0.7975	5.3264
		2	40	0.8867	0.7972	5.6194
	ROSE	0	0	0.8305	0.7103	6.1316
		1	20	0.8414	0.7264	5.9551
		2	40	0.8435	0.7296	6.0193
FAZ	OCTA-500(3M)	0	0	0.9545	0.9345	3.2943
		1	5	0.9800	0.9586	2.3500
		2	5	0.9838	0.9692	2.2432
	OCTA-500(6M)	0	0	0.8787	0.7991	3.4278
		1	5	0.9042	0.8402	3.2013
		2	5	0.9073	0.8473	3.3271
	ROSE	0	0	0.9495	0.8996	3.3078
		1	5	0.9717	0.9452	2.8669
		2	5	0.9712	0.9442	2.8612
Capillary	OCTA-500(3M)	0	0	0.8790	0.7845	7.4955
		1	30	0.8794	0.7851	7.5338
		2	60	0.8785	0.7837	7.6070
	OCTA-500(6M)	0	0	0.8354	0.7175	9.2106
		1	45	0.8349	0.7171	9.0373
		2	90	0.8373	0.7204	8.9759
	ROSE	0	0	0.7496	0.6012	7.4011
		1	20	0.7548	0.6076	7.5559
		2	40	0.7586	0.6129	7.5746
Artery	OCTA-500(3M)	0	0	0.8342	0.7528	4.5124
		1	25	0.8633	0.7687	4.3201
		2	45	0.8747	0.7785	4.1428
	OCTA-500(6M)	0	0	0.8352	0.7325	5.2439
		1	30	0.8503	0.7432	5.2781
		2	55	0.8602	0.7572	5.0621
Vein	OCTA-500(3M)	0	0	0.8409	0.7463	4.4990
		1	25	0.8719	0.7746	3.7448
		2	45	0.8817	0.7897	3.6399
	OCTA-500(6M)	0	0	0.8263	0.7168	5.4879
		1	30	0.8357	0.7219	4.9593
		2	55	0.8526	0.7474	4.9144

of introducing more prompt points is quite limited; segmentation performance relies more on the image encoder's comprehension of image features. In the label of capillary, there is a significant difference in the distribution of vessels between the lesion and normal samples. Therefore, more prompt points are considered. Nevertheless, the segmentation performance gap between using prompt points and not using them remains small. However, due to the potent global

image feature extraction capability of ViT and the well-pre-trained weights of SAM, the resulting vessel segmentation is still good. Users can obtain reasonably accurate results without prompt point inputs when practically performing RV and capillary segmentation in global mode.

In contrast, it can be inferred from Table 2 that including prompt points results in a more substantial improvement in FAZ segmentation. From some examples shown in Figure 6 and the features of FAZ, it can be inferred that these targets

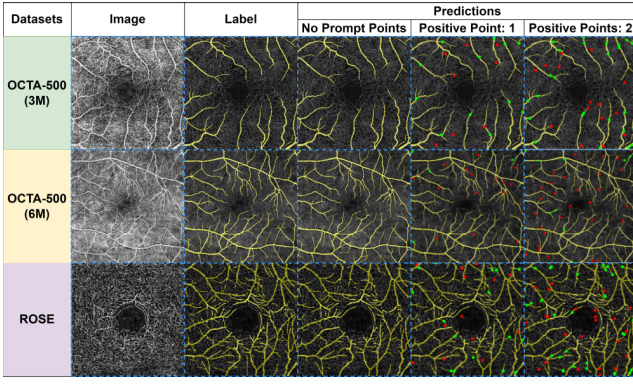


Figure 4: The segmentation result of RV in global mode.

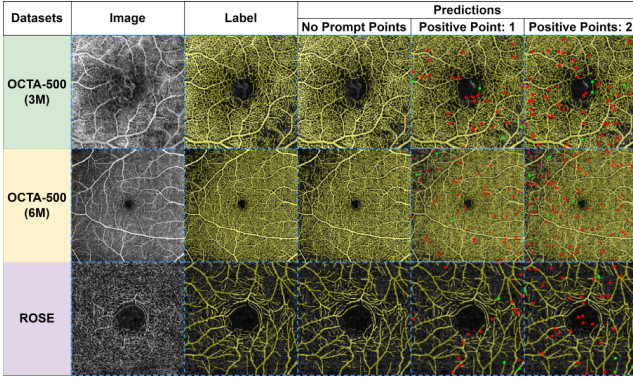


Figure 5: The segmentation result of capillary in global mode.

have relatively fixed positions and well-defined boundaries, making the information from prompt points crucial. SAM can accurately localize segmentation targets without prompt points but struggles to distinguish segmentation boundaries. The addition of prompt points effectively addresses this issue.

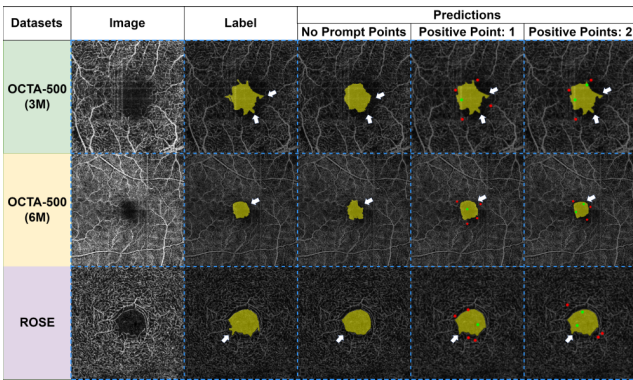


Figure 6: The segmentation result of FAZ in global mode. The areas indicated by the arrows represent the improvement in the segmentation boundary after adding prompt points.

Table 3 compares the performance of different methods on RV and FAZ segmentation metrics in the OCTA-500 dataset. Initially, only FAZ and RV annotations were available for the OCTA-500 dataset, so many studies only conducted experiments on these two tasks. The experimental data from previous methods are referenced from Hu et al. (2022b); Masset (2000). Our method's comprehensive performance reaches the state-of-the-art level. Comparing the last two rows, it can be observed that there is a significant improvement in SAM after fine-tuning. The necessity of fine-tuning is demonstrated. Without fine-tuning, the performance of vessel segmentation tasks is lower than that of FAZ segmentation. The reason for this can be inferred as FAZ being a single and completed segmentation target. It is easier to segment, and its shape is closer to the data used for SAM's pre-training.

Artery and vein segmentation need to be analyzed in conjunction. The result is presented in 2 and Figure 7. It can be discerned from the labels that the union of arteries and veins in OCTA images constitutes the RVs. In contrast to RV segmentation, in AV segmentation, the role of prompt points is quite substantial despite the morphological similarity. For the model, it is important to determine the shape boundaries and types of the vessels. Without prompt points, distinguishing between different types of vessels is challenging, which is a major reason for the obvious disparities in metrics and noticeable image segmentation errors. Aside from the similar morphology, two additional factors cause difficulty in discriminating vessel types. One factor is that neighboring arteries and veins can be interconnected or overlap. It is hard to discern the boundaries of the targets, resulting in segmentation results with overflow or discontinuities. Another factor is the presence of some pathological samples where vessels are missing or distorted. In such cases, relying on the relative positions of vessels to determine their types is problematic. Marking negative points on adjacent non-target vessels effectively addresses the issues caused by the two factors mentioned above, improving segmentation results.

4.3.2. Local Mode

The local mode primarily focuses on precisely segmenting vessels in local regions. The vessel is discerned and segmented more precisely using prompt points from SAM. The segmentation targets include RV, artery, and vein. This work is currently exploratory, as there have been no similar studies to date. We selected a connected component and its surrounding region for each sample to extract prompt points. The experimental results are summarized in Table 4.

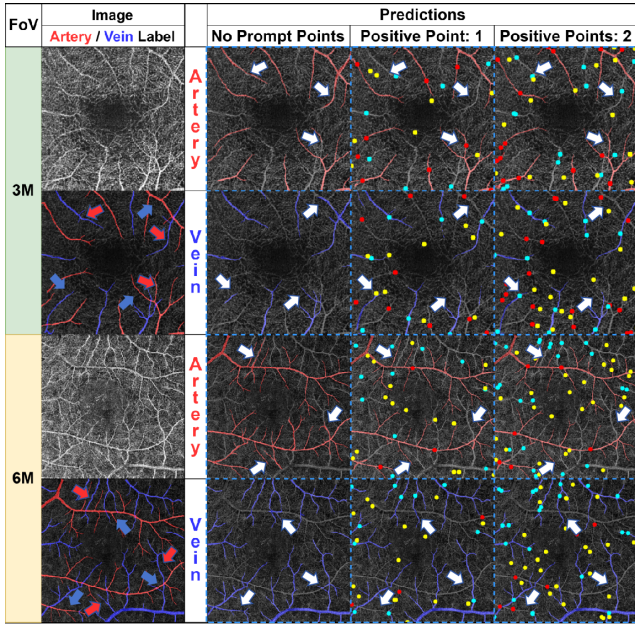
The SAM can produce reasonable segmentation results in the global mode without prompt point input for the prompt encoder. The absence of prompt point input in the local mode leads to ambiguity. In the initial attempts, we addressed this issue by cropping the original images. A more detailed description of the experiments regarding the cropping approach is provided in Appendix .

The main purpose of RV segmentation is to attempt to determine the feasibility of this approach and observe the

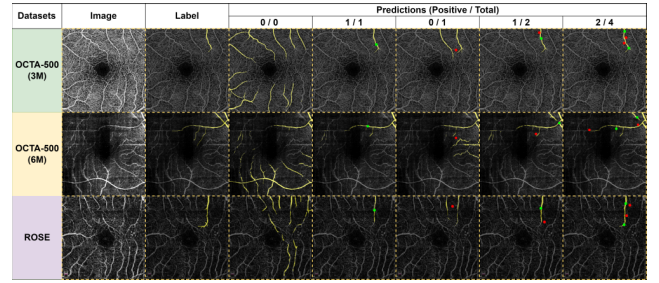
Table 3

RV and FAZ segmentation results on OCTA-500 dataset (underscores indicate the top two highest values).

Method	RV			FAZ								
	OCTA-500(3M)			OCTA-500(6M)			OCTA-500(3M)			OCTA-500(6M)		
	Dice ↑	Jaccard ↑	HD ↓	Dice ↑	Jaccard ↑	HD ↓	Dice ↑	Jaccard ↑	HD ↓	Dice ↑	Jaccard ↑	HD ↓
U-Net (2015)	0.9068	0.8301	<u>3.20</u>	0.8876	0.7987	<u>4.98</u>	0.9747	0.9585	4.85	0.8770	0.8124	<u>6.40</u>
IPN (2020)	0.9062	0.8325	-	0.8864	0.7973	-	0.9505	0.9091	-	0.8802	0.7980	-
IPN V2+ (2021)	<u>0.9274</u>	<u>0.8667</u>	-	<u>0.8941</u>	<u>0.8095</u>	-	0.9755	0.9532	-	<u>0.9084</u>	0.8423	-
FARGO (2021)	0.9112	0.8374	<u>2.78</u>	0.8798	0.7864	<u>4.47</u>	0.9785	0.9587	<u>3.11</u>	0.8930	0.8355	7.76
Joint-Seg (2022)	0.9113	0.8378	-	<u>0.8972</u>	<u>0.8117</u>	-	<u>0.9843</u>	<u>0.9693</u>	-	0.9051	<u>0.8424</u>	-
SAM (not fine-tuned)	0.5366	0.3730	8.94	0.3101	0.1889	10.76	0.9221	0.8600	3.64	0.7802	0.6750	4.13
SAM-OCTA (ours)	<u>0.9199</u>	<u>0.8520</u>	4.11	0.8869	0.7975	5.32	<u>0.9838</u>	<u>0.9692</u>	<u>2.24</u>	<u>0.9073</u>	<u>0.8473</u>	<u>3.20</u>


Figure 7: The artery-vein segmentation result in global mode. As the number of prompt points increases, the segmentation performance improves. The arrows point out the improved regions.

potential impact of prompt points in this mode. Due to the contact between arteries and veins, the segmentation targets may not be a single vessel. From Table 4 and Figure 8, it could be found that one positive prompt point is enough to eliminate the ambiguity effectively. Once the positions of the connected components are determined, adding more prompt points becomes less influential in segmentation improvement. The case with a single negative prompt point was also tested, and when it is placed between two vessels, the ambiguity issue still persists. However, the segmentation region is clearer than the case without prompt points. Unsimilar to the global mode, the impact of prompt points on segmentation performance varies for images with different FoVs in the local mode. When the FoV is 6M, due to the wider vision, two large arteries located above and below the FAZ are


Figure 8: The segmentation result of RV in local mode.

often included in the image (the arteries could be found in Figure 10(a)). The distribution of the vessels is extensive in the image, and sometimes, segmentation can fail with just a single positive prompt point, especially in cases with artifact images. It is the reason why prompt points provide more assistance in segmentation for 6M FoV images.

The results of artery-vein segmentation in the local mode are shown in Table 4 and Figure 9. Like the RV segmentation, the positive prompt points impact segmentation performance more than the negative. When arteries and veins overlap, it is challenging to effectively differentiate between them with a single-type prompt point. This characteristic is the same as the artery-vein segmentation in the global mode. Several prompt points are sufficient to achieve good segmentation results. Even in cases where different types of vessels overlap in multiple locations, the model can effectively distinguish and segment them.

5. Discussion

5.1. Number of Prompt Points

The discussion regarding the number of prompt points concerns selecting the total prompt points number for segmentation tasks in the global mode. As mentioned in Section 4.3.1, the total number of prompt points should be the same for each sample. Table 5 records the maximum connected components for each sample in different labels. The total number of feature points is aligned with this value rounded

Table 4

Segmentation results for the local mode.

Label	Dataset	Prompt Points		Dice ↑	Jaccard ↑	HD ↓
		Positive	Total			
RV	OCTA-500(3M)	0	0	0.1168	0.0332	3.6368
		1	0	0.8821	0.7965	1.9123
		0	1	0.6496	0.5590	3.0018
		1	1	0.8902	0.8105	2.1627
		2	2	0.8884	0.8054	2.1928
	OCTA-500(6M)	0	0	0.1602	0.1083	9.5724
		1	0	0.7061	0.5844	4.1282
		0	1	0.5653	0.4448	4.7569
		1	1	0.7844	0.6594	3.3035
		2	2	0.8128	0.6914	3.1239
	ROSE	0	0	0.1229	0.0988	10.235
		1	0	0.6457	0.4885	3.4124
		0	1	0.4512	0.3231	5.2034
		1	1	0.6590	0.5070	3.2051
		2	2	0.6866	0.5266	3.2792
Artery	OCTA-500(3M)	1	1	0.8459	0.7546	2.4934
		0	1	0.8041	0.7056	2.6959
		1	2	0.8736	0.7953	2.3998
		2	4	0.9097	0.8356	2.0340
	OCTA-500(6M)	1	1	0.7450	0.6243	3.2347
		0	1	0.6507	0.5403	3.2520
		1	2	0.7713	0.6519	2.9656
		2	4	0.8066	0.6943	2.6347
Vein	OCTA-500(3M)	1	1	0.8250	0.7311	2.0093
		0	1	0.7859	0.6918	2.0144
		1	2	0.8495	0.7583	1.9965
		2	4	0.8718	0.7833	1.9018
	OCTA-500(6M)	1	0	0.7507	0.6327	2.7928
		0	1	0.6575	0.5459	2.9790
		1	2	0.7819	0.6661	2.7831
		2	4	0.8044	0.6898	2.6247

up to the nearest multiple of 5 or 10. Considering that even in the case of a sample with the largest connected component number, some negative points must be included.

For the FAZ, it appears as a whole region in the center of the OCTA images, and its connected components' number is fixed at 1. However, there is a considerable difference in the number of connected components among different samples of vessels. The selected relative positioning, individual variations, and pathological conditions may influence the number. Figure 10 illustrates two samples with obvious differences in the number of connected components under the same FoV. Interestingly, experimental results have shown that the effect of prompt points is minimal for RV and capillary segmentation in the global mode. Therefore, despite the large number of negative prompt points in the example images, they are not essential for the actual segmentation task. Since positive and negative points can be exchanged based on the segmentation target for artery-vein segmentation, they should be merged and counted together.

Table 5

Max connected components count.

Dataset	Label			
	RV	Capillary	FAZ	Artery + Vein
OCTA-500(3M)	19	29	1	22
OCTA-500(6M)	18	44	1	27
ROSE	29	20	1	-

5.2. Applicability of Prompt Points

In OCTA segmentation tasks, the applicability of prompt points is manifested in two aspects. On one aspect, prompt points serve the purpose of localizing the segmentation targets, forming the foundation for segmentation in the local mode. For instance, in the case of RV segmentation under the local mode, marking a positive point improves segmentation performance, while adding more prompt points has only a slight impact. Hence, segmentation in the local mode

FoV	Image	Artery / Vein Label	Predictions (Positive / Total)			
			1 / 1	0 / 1	1 / 2	2 / 4
3M		Artery				
		Vein				
6M		Artery				
		Vein				

Figure 9: The segmentation result of artery-vein in local mode.

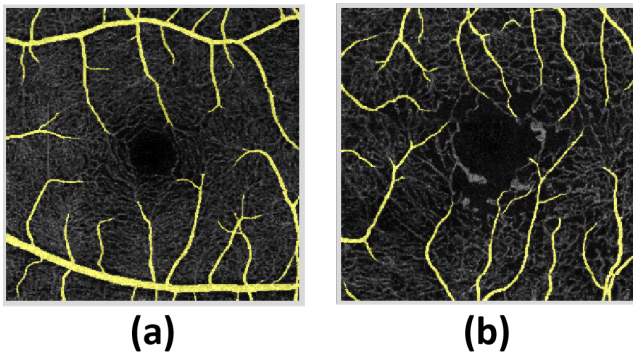


Figure 10: Examples of connected components in the OCTA-500 dataset samples. (a) Normal sample, age 13, with three connected components; (b) Diabetic retinopathy sample, age 48, with 17 connected components.

can be considered a combination of segmentation as in the global mode and enhancing target localization through prompt points.

Prompt points also enhance segmentation boundaries, which is evident in FAZ and artery-vein. In FAZ, some prompt points on the edges help the model determine the shape's degree of dilation and contraction. For arteries and veins, prompt points aid in avoiding incorrect vessel type recognition and optimizing segmentation boundaries at artery-vein junctions.

6. Conclusion

This paper utilizes the LoRA technique and proposes a prompt points generation approach to fine-tune SAM for segmentation tasks based on OCTA datasets. Our method is named SAM-OCTA, which achieves or approaches the SoTA results in multiple OCTA image segmentation tasks and a detailed analysis is conducted of the effect of prompt

points in multiple tasks. This method performs well in conventional OCTA segmentation tasks (RV and FAZ) and yields favorable outcomes in segmenting capillary, artery, and vein targets.

As a fine-tuning strategy, SAM-OCTA freezes the original parameters of SAM, thus preserving its existing powerful image semantic comprehension capabilities. It is the reason that SAM has some competence in FAZ segmentation without fine-tuning. However, fine-tuning is still essential for further improvement in segmentation performance. Fine-tuning serves a dual purpose: firstly, it helps the image encoder adapt to the unique OCTA image type; secondly, it facilitates the integration of the image and the prompt point features.

A strategy based on target annotation and connected components generation is adopted for prompt points. The reason for involving label information is to consider that if users provide prompt points when using relevant segmentation tools in practice, they will implicitly incorporate their perceived ground-truth expectation. The effect of prompt points varies for different segmentation tasks. For RV and capillary segmentation, the influence is subtle. It takes a moderate improvement for FAZ, but it is crucial for artery-vein segmentation.

The artery-vein segmentation with SAM-OCTA was also explored. With prompt point information, artery-vein segmentation has achieved better results than the previous supervised methods. Furthermore, we conduct experiments on the segmentation of vessels in local regions and achieved promising results. This exploratory work aims to assist users in segmenting OCTA vascular targets of their specific interest. SAM-OCTA is expected to be an effective tool for diagnosing OCTA-related diseases, especially those involving artery-vein lesion structures.

Declaration of Competing Interest

The authors declare that they have no known competing financial interests or personal relationships that could have appeared to influence the work reported in this paper.

Declaration of Competing Interest

The data is publicly available, and the code has been public on GitHub.

Acknowledgement

This work is supported by the Chongqing Technology Innovation Application Development Key Project (cstc2020jscx; dxwtBX0055; cstb2022tiad-kpx0148).

CRedit authorship contribution statement

Xinrun Chen: Methodology, Software, Writing. **Chengliang Wang:** Conceptualization of this study. **Haojian Ning:** Data curation and analysis. **Shiying Li:** Medical advisor.

References

- Alam, M., Le, D., Son, T., Lim, J.I., Yao, X., 2020. Av-net: deep learning for fully automated artery-vein classification in optical coherence tomography angiography. *Biomedical optics express* 11, 5249–5257.
- Breger, A., Goldbach, F., Gerendas, B.S., Schmidt-Erfurth, U., Ehler, M., 2022. Blood vessel segmentation in en-face octa images: a frequency based method, in: *Medical Imaging 2022: Computer-Aided Diagnosis*, SPIE. pp. 520–530.
- Buslaev, A., Iglovikov, V.I., Khvedchenya, E., Parinov, A., Druzhinin, M., Kalinin, A.A., 2020. Albumentations: Fast and flexible image augmentations. *Information* 11. URL: <https://www.mdpi.com/2078-2489/11/2/125>, doi:10.3390/info11020125.
- Cheng, D., Qin, Z., Jiang, Z., Zhang, S., Lao, Q., Li, K., 2023. Sam on medical images: A comprehensive study on three prompt modes. *arXiv preprint arXiv:2305.00035*.
- Cheung, C.Y., Ikram, M.K., Klein, R., Wong, T.Y., 2015. The clinical implications of recent studies on the structure and function of the retinal microvasculature in diabetes. *Diabetologia* 58, 871–885.
- Cheung, C.Y.I., Sabanayagam, C., Law, A.K.p., Kumari, N., Ting, D.S.w., Tan, G., Mitchell, P., Cheng, C.Y., Wong, T.Y., 2017. Retinal vascular geometry and 6 year incidence and progression of diabetic retinopathy. *Diabetologia* 60, 1770–1781.
- Dosovitskiy, A., Beyer, L., Kolesnikov, A., Weissenborn, D., Zhai, X., Unterthiner, T., Dehghani, M., Minderer, M., Heigold, G., Gelly, S., et al., 2020. An image is worth 16x16 words: Transformers for image recognition at scale. *arXiv preprint arXiv:2010.11929*.
- Hao, J., Shen, T., Zhu, X., Liu, Y., Behera, A., Zhang, D., Chen, B., Liu, J., Zhang, J., Zhao, Y., 2022. Retinal structure detection in octa image via voting-based multitask learning. *IEEE Transactions on Medical Imaging* 41, 3969–3980.
- He, K., Fan, H., Wu, Y., Xie, S., Girshick, R., 2020. Momentum contrast for unsupervised visual representation learning, in: *Proceedings of the IEEE/CVF conference on computer vision and pattern recognition*, pp. 9729–9738.
- Hu, E.J., Shen, Y., Wallis, P., Allen-Zhu, Z., Li, Y., Wang, S., Wang, L., Chen, W., 2021. Lora: Low-rank adaptation of large language models. *arXiv preprint arXiv:2106.09685*.
- Hu, J., Wang, H., Wu, G., Cao, Z., Mou, L., Zhao, Y., Zhang, J., 2022a. Multi-scale interactive network with artery/vein discriminator for retinal vessel classification. *IEEE Journal of Biomedical and Health Informatics* 26, 3896–3905.
- Hu, K., Jiang, S., Zhang, Y., Li, X., Gao, X., 2022b. Joint-seg: Treat foveal avascular zone and retinal vessel segmentation in octa images as a joint task. *IEEE Transactions on Instrumentation and Measurement* 71, 1–13.
- Ke, L., Ye, M., Danelljan, M., Liu, Y., Tai, Y.W., Tang, C.K., Yu, F., 2023. Segment anything in high quality. *arXiv preprint arXiv:2306.01567*.
- Kirillov, A., Mintun, E., Ravi, N., Mao, H., Rolland, C., Gustafson, L., Xiao, T., Whitehead, S., Berg, A.C., Lo, W.Y., et al., 2023. Segment anything. *arXiv preprint arXiv:2304.02643*.
- Li, M., Chen, Y., Ji, Z., Xie, K., Yuan, S., Chen, Q., Li, S., 2020a. Image projection network: 3d to 2d image segmentation in octa images. *IEEE Transactions on Medical Imaging* 39, 3343–3354.
- Li, M., Zhang, Y., Ji, Z., Xie, K., Yuan, S., Liu, Q., Chen, Q., 2020b. Ipn-v2 and octa-500: Methodology and dataset for retinal image segmentation. *arXiv preprint arXiv:2012.07261*.
- Li, W., Zhang, H., Li, F., Wang, L., 2022a. Rps-net: An effective retinal image projection segmentation network for retinal vessels and foveal avascular zone based on octa data. *Medical Physics* 49, 3830–3844.
- Li, Y., Zeghlache, R., Brahim, I., Xu, H., Tan, Y., Conze, P.H., Lamard, M., Quéllec, G., El Habib Dahou, M., 2022b. Segmentation, classification, and quality assessment of uw-octa images for the diagnosis of diabetic retinopathy, in: *MICCAI Challenge on Mitosis Domain Generalization*. Springer, pp. 146–160.
- Liang, Z., Zhang, J., An, C., 2021. Foveal avascular zone segmentation of octa images using deep learning approach with unsupervised vessel segmentation, in: *ICASSP 2021-2021 IEEE International Conference on Acoustics, Speech and Signal Processing (ICASSP)*, IEEE. pp. 1200–1204.
- Liu, J., He, L., Kang, Y., Zhuang, Z., Wang, D., Xu, H., 2023. Ceil: Generalized contextual imitation learning. *arXiv preprint arXiv:2306.14534*.
- Liu, J., Shen, H., Wang, D., Kang, Y., Tian, Q., 2021. Unsupervised domain adaptation with dynamics-aware rewards in reinforcement learning. *Advances in Neural Information Processing Systems* 34, 28784–28797.
- López-Varela, E., de Moura, J., Novo, J., Fernández-Vigo, J.I., Moreno-Morillo, F.J., Ortega, M., 2023. Fully automatic segmentation and monitoring of choriocapillaris flow voids in octa images. *Computerized Medical Imaging and Graphics* 104, 102172.
- Ma, Y., Hao, H., Xie, J., Fu, H., Zhang, J., Yang, J., Wang, Z., Liu, J., Zheng, Y., Zhao, Y., 2020. Rose: a retinal oct-angiography vessel segmentation dataset and new model. *IEEE transactions on medical imaging* 40, 928–939.
- Ma, Y., Yan, Q., Liu, Y., Liu, J., Zhang, J., Zhao, Y., 2023. Strunet: Perceptual and low-rank regularized transformer for medical image denoising. *Medical Physics*.
- Ma, Z., Feng, D., Wang, J., Ma, H., 2022. Retinal octa image segmentation based on global contrastive learning. *Sensors* 22, 9847.
- Masset, F., 2000. Fargo: A fast eulerian transport algorithm for differentially rotating disks. *Astronomy and Astrophysics Supplement Series* 141, 165–173.
- Meiburger, K.M., Salvi, M., Rotunno, G., Drexler, W., Liu, M., 2021. Automatic segmentation and classification methods using optical coherence tomography angiography (octa): a review and handbook. *Applied Sciences* 11, 9734.
- Mishra, S., Wang, Y.X., Wei, C.C., Chen, D.Z., Hu, X.S., 2021. Vtgn-net: a cnn based vessel topology graph network for retinal artery/vein classification. *Frontiers in Medicine* 8, 750396.
- Peng, Z., Xu, Z., Zeng, Z., Yang, X., Shen, W., 2023. Sam-parser: Fine-tuning sam efficiently by parameter space reconstruction. *arXiv preprint arXiv:2308.14604*.
- Radford, A., Kim, J.W., Hallacy, C., Ramesh, A., Goh, G., Agarwal, S., Sastry, G., Askell, A., Mishkin, P., Clark, J., et al., 2021. Learning transferable visual models from natural language supervision, in: *International conference on machine learning*, PMLR. pp. 8748–8763.
- Seidemann, S.B., Claggett, B., Bravo, P.E., Gupta, A., Farhad, H., Klein, B.E., Klein, R., Di Carli, M., Solomon, S.D., 2016. Retinal vessel calibers in predicting long-term cardiovascular outcomes: the atherosclerosis risk in communities study. *Circulation* 134, 1328–1338.
- Shi, P., Qiu, J., Abaxi, S.M.D., Wei, H., Lo, F.P.W., Yuan, W., 2023a. Generalist vision foundation models for medical imaging: A case study of segment anything model on zero-shot medical segmentation. *Diagnostics* 13, 1947.
- Shi, Z., Li, Y., Zou, H., Zhang, X., 2023b. Tcu-net: Transformer embedded in convolutional u-shaped network for retinal vessel segmentation. *Sensors* 23, 4897.
- Shit, S., Paetzold, J.C., Sekuboyina, A., Ezhov, I., Unger, A., Zhylka, A., Pluim, J.P., Bauer, U., Menze, B.H., 2021. cldice-a novel topology-preserving loss function for tubular structure segmentation, in: *Proceedings of the IEEE/CVF Conference on Computer Vision and Pattern Recognition*, pp. 16560–16569.
- Tan, X., Chen, X., Meng, Q., Shi, F., Xiang, D., Chen, Z., Pan, L., Zhu, W., 2023. Oct2former: A retinal oct-angiography vessel segmentation transformer. *Computer Methods and Programs in Biomedicine* 233, 107454.
- Vali, M., Nazari, B., Sadri, S., Pour, E.K., Riazi-Esfahani, H., Faghihi, H., Ebrahimiadib, N., Azizkhani, M., Innes, W., Steel, D.H., et al., 2023. Cnv-net: Segmentation, classification and activity score measurement of choroidal neovascularization (cnv) using optical coherence tomography angiography (octa). *Diagnostics* 13, 1309.
- Wang, C., Ning, H., Chen, X., Li, S., 2023. Db-unet: Mlp based dual branch unet for accurate vessel segmentation in octa images, in: *ICASSP 2023-2023 IEEE International Conference on Acoustics, Speech and Signal Processing (ICASSP)*, IEEE. pp. 1–5.
- Wang, Y., Shen, Y., Yuan, M., Xu, J., Yang, B., Liu, C., Cai, W., Cheng, W., Wang, W., 2021. A deep learning-based quality assessment and segmentation system with a large-scale benchmark dataset for optical coherence

- tomographic angiography image. arXiv preprint arXiv:2107.10476 .
- Wu, X., Gao, D., Williams, B.M., Stylianides, A., Zheng, Y., Jin, Z., 2020. Joint destriping and segmentation of octa images, in: Medical Image Understanding and Analysis: 23rd Conference, MIUA 2019, Liverpool, UK, July 24–26, 2019, Proceedings 23, Springer. pp. 423–435.
- Zhang, C., Liu, L., Cui, Y., Huang, G., Lin, W., Yang, Y., Hu, Y., 2023. A comprehensive survey on segment anything model for vision and beyond. arXiv preprint arXiv:2305.08196 .
- Zhang, K., Liu, D., 2023. Customized segment anything model for medical image segmentation. arXiv preprint arXiv:2304.13785 .
- Zhang, Y., Jiao, R., 2023. How segment anything model (sam) boost medical image segmentation? arXiv preprint arXiv:2305.03678 .
- Zhu, C., Wang, H., Xiao, Y., Dai, Y., Liu, Z., Zou, B., 2022. Ovs-net: An effective feature extraction network for optical coherence tomography angiography vessel segmentation. Computer Animation and Virtual Worlds 33, e2096.

Appendix

A. Local Mode with Cropped Images

This section will explain an exploratory experiment on artery-vein segmentation, which can be considered a local mode without prompt points. From the results of RV segmentation in the local mode, it is evident that segmenting specific connected components leads to ambiguity without prompt points. Initially, we were unaware of the role of prompt points in localization, so we employed a cropping approach before segmentation.

The approach can be represented as Figure 11. We first identify the bounding box of the desired connected component to be segmented and then round its width and height ranges up to $\frac{1}{4}$, $\frac{1}{2}$, $\frac{3}{4}$, and 1 of the image width. Then, cropping the image and resizing it to the original size. The purpose is to maintain the aspect ratio of the images. Next, similar to the global mode, different numbers of prompt points were selected for fine-tuning, and the results were recorded and observed.

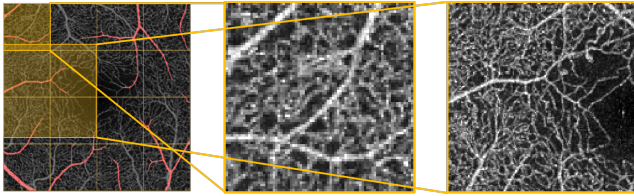


Figure 11: Image cropping in the local mode.

Table 6 and Figure 12 present the experimental results of this strategy. It can be observed that with an increase in the number of prompt points, the segmentation performance improves. This also reaffirms the role of prompt points in optimizing segmentation boundaries.

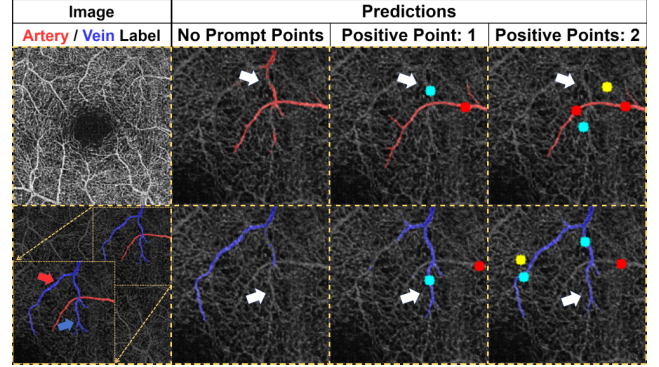


Figure 12: Results of Artery-vein Segmentation with Cropped Images.

Table 6

Segmentation results in local mode with cropped images.

Label	Dataset	Prompt Points		Dice ↑	Jaccard ↑	HD ↓
		Positive	Total			
Artery	3M	0	0	0.7393	0.6339	2.0765
		1	2	0.8540	0.7576	1.9010
		2	4	0.8707	0.7792	1.8148
	6M	0	0	0.6865	0.5699	4.3822
		1	2	0.7718	0.6649	3.7610
		2	4	0.7922	0.6851	3.5811
Vein	3M	0	0	0.7742	0.6658	2.4864
		1	2	0.8007	0.6921	2.4388
		2	4	0.8352	0.7267	2.3226
	6M	0	0	0.7053	0.5823	2.9789
		1	2	0.8046	0.6833	2.7781
		2	4	0.8167	0.7014	2.7174